Article

Structure and biomechanics during xylem vessel transdifferentiation in *Arabidopsis thaliana*

Eleftheria Roumeli [1,2,*,‡], Leah Ginsberg [2,‡], Robin McDonald[2], Giada Spigolon[3], Rodinde Hendrickx[2], Misato Ohtani[4,5], Taku Demura[5], Guruswami Ravichandran[2], Chiara Daraio[2]

1 Department of Materials Science and Engineering, University of Washington, Seattle, WA 98195
2 Division of Engineering and Applied Science, California Institute of Technology, Pasadena, California 91125, United States
3 Biological Imaging Facility, California Institute of Technology, Pasadena, California 91125, United States
4 Department of Integrated Biosciences, Graduate School of Frontier Sciences, The University of Tokyo, Kashiwa, 277-8562, Japan
5 Graduate School of Biological Sciences, Nara Institute of Science and Technology, Takayama 8916-5, Ikoma, Nara 630-0192, Japan
* Correspondence: eroumeli@uw.edu
‡ These authors contributed equally to this work.

Abstract: Individual plant cells are the building blocks for all plantae and artificially constructed plant biomaterials, like biocomposites. Secondary cell walls (SCWs) are a key component for mediating mechanical strength and stiffness in both living vascular plants and biocomposite materials. In this paper, we study the structure and biomechanics of cultured plant cells during the cellular developmental stages associated with SCW formation. We use a model culture system that induces transdifferentiation of *Arabidopsis thaliana* cells to xylem vessel elements, upon treatment with dexamethasone (DEX). We group the transdifferentiation process into three distinct stages, based on morphological observations of the cell walls. The first stage includes cells with only a primary cell wall (PCW), the second covers cells that have formed a SCW, and the third stage includes cells with a ruptured tonoplast and partially or fully degraded PCW. We adopt a multi-scale approach to study the mechanical properties of cells in these three stages. We perform large-scale indentations with a micro-compression system and nanoscale indentations through atomic force microscopy (AFM), in three different osmotic conditions. We introduce a spring-based model to deconvolve the competing stiffness contributions from turgor pressure, PCW, SCW and cytoplasm in the stiffness of differentiating cells. Prior to triggering differentiation, cells in hypotonic pressure conditions are significantly stiffer than cells in isotonic or hypertonic conditions, highlighting the dominant role of turgor pressure. Plasmolyzed cells with a SCW reach similar levels of stiffness as cells with maximum turgor pressure. The stiffness of the PCW in all of these conditions is lower than the stiffness of the fully-formed SCW. Our results provide the first experimental characterization of the mechanics of SCW formation at single cell level.

Keywords: Plant biomechanics; turgor pressure; micro-compression; AFM; *Arabidopsis thaliana*; differentiation

1. Introduction

Plantae and plant-based materials are specialized conglomerates of plant cells. Therefore, studying the mechanical properties of single cells and resolving further sub-cellular contributions provides a basis for further analysis of the heterogeneous tissue and plant-level biomechanics. In vascular plant tissues, the micro-structure and composition of secondary cell wall (SCW) governs, to a large extent, the mechanical properties of the entire tissue [1,2]. Thus, it is of paramount importance to investigate the mechanical properties of the SCW, especially during the initial stages of formation, which has not been explored to date.

 doi:10.20944/preprints202011.0188.v1

Plant cells have two key structural elements that collectively govern their mechanical properties: the cell wall and the cytoskeleton. The key structural component of the cell wall is cellulose, which has a Young's modulus ($E = 110 - 220$ GPa) comparable to that of high performance engineering materials like carbon fiber or steel [3]. Cellulose is immersed in an amorphous matrix of softer biopolymers, hemicellulose, pectin, proteins and lignin, giving rise to a complex heterogeneous multilayered cell wall structure [4]. The support provided to plant cells by the cell wall allows them to hold water at high pressures ($p = 0.3 - 1.0$ MPa), mainly through swelling of the vacuole [5]. This phenomenon in plants is known as turgor pressure, and it is essential to the structural integrity and rigidity of the cell. Additional structural support is provided to the cell by the cytoskeleton, largely through actin filaments ($E = 1.0 - 4.0$ kPa) and microtubules ($E = 1.1 - 1.3$ GPa) [6–8].

Recent advances in instrumentation are the impetus for the resurgence in research focused on the mechanics of cell growth [9–11]. Newly designed experiments have the potential to achieve an unprecedented spatial resolution and therefore to decouple the mechanical contributions from each structural element of a cell in the overall mechanical performance of plant cells and tissues. Experimental methods, protocols and mechanical models of plant cells vary, contributing to results that span orders of magnitude [9]. Routier-Kierzkowska et al. designed an experimental apparatus which they termed as cellular force microscope (CFM) and used it to create stiffness maps of onion epidermis peels [12]. They found that the tissue was softer over the junctions between cell walls than over the top of an inflated (turgid) cell. In the leaves of *Arabidopsis thaliana* (Arabidopsis) plants, particularly in epithelial cells, it was found that there is a direct correlation between microtubule (MT) organization and geometry-derived mechanical stresses [13]. Apparently, the maximum stress in the cell wall is found in areas with highest cellulose concentration, which is driven by the MTs in the cytoplasm. Finite-element simulations revealed that turgor pressure caused the observed stiffening on top of inflated cells. Radotić et al. performed AFM indentation measurements on suspension-cultured Arabidopsis cells and observed that the cell wall stiffness at the beginning and end of cell growth was almost an order of magnitude lower than during the exponential growth phase [14]. This finding is consistent with cell wall loosening behavior in preparation or during cell elongation, as explained by Cosgrove in a later review [4]. Braybrook and Peaucelle performed AFM indentations on plasmolyzed Arabidopsis tissues to ensure isolation of the response of the cell wall from any contribution due to turgor pressure [15]. By measuring the response from the plasmolyzed tissue, they were able to demonstrate that auxin leads to wall acidification in preparation for cell expansion. This finding is, again, consistent with cell wall loosening behavior in preparation for cell elongation. Durand-Smet et al. used a micro-rheometer to measure the elastic and loss moduli of isolated Arabidopsis protoplasts [8]. They found that the elastic modulus of the protoplast was about three orders of magnitude lower than plant cells with a cell wall. They also treated plant cells with a microtubule destabilizing drug, which reduced the elastic modulus of the protoplast to half of its original value, demonstrating that MTs contribute to the overall stiffness of the cell. Even though many are working towards a defined micromechanical model, the exact contribution of the cell wall(s) and cytoplasm on the effective stiffness of the system during growth and differentiation remains elusive. Here, in order to understand the contributions of the subcellular components in the mechanical properties of plant cells, we propose a robust multi-scale mechanics assay that includes nano-indentation to capture cell wall properties, chemical treatments to control osmotic conditions and micro-indentation to evaluate global cell properties.

We choose to focus on xylem vessel element differentiation, which is one of the most extensively used systems to study SCW development and thickening [16,17]. Xylem vessel elements develop a precisely patterned SCW beneath the primary cell wall (PCW) giving rise to an entangled multilayered heterostructure. The deposition of SCW in xylem vessel elements is intricately linked to programmed cell death (PCD), and both processes are happening concurrently during the differentation. Therefore, quantifying the mechanical contributions of the cell wall(s) and cytoplasm during differentiation of xylem vessel elements is a convoluted problem, and one that has not yet been solved. Our multi-scale

 doi:10.20944/preprints202011.0188.v1

biomechanical assay is designed to capture mechanical contributions from the PCW, the SCW, their potential coupled effects, as well as the cytoskeleton at various turgor pressures and osmotic conditions. To our knowledge this is the first time such an extensive biomechanics assay has been employed to study plant cell behavior.

Common morphological observations during differentiation of tracheary elements (TEs) in *Zinnia elegans*, *Populus deltoides* and Arabidopsis, in the order that they occur, are: (i) the differentiating cell expands, becoming highly vacuolated and the nucleus becomes confined, pushing against the cell wall; (ii) the cell produces vesicles which have been associated with substance exchange between the cytoplasm and cell wall for SCW deposition; (iii) tonoplast ruptures upon SCW synthesis; (iv) following SCW deposition, in planta, PCW perforation is observed [18–20].

Early in vitro SCW induction systems for *Zinnia elegans* facilitated physiological, biochemical, and molecular studies that elucidated the TE differentiation mechanism [21–23]. The Demura group introduced the post-translational induction system of VASCULAR-RELATED NAC-DOMAIN7 (VND7) genes which induces transdifferentiation of various types of plant cells into xylem vessel elements upon treatment with a glucocorticoid, such as dexamethasone (DEX) [16,17]. The induction system has been demonstrated successfully in Arabidopsis plants and cell cultures, as well as *Populus tremula x tremuloides* plantlets, and *Nicotiana tabacum* cell cultures [16]. The system causes the activation of transcriptional activity of VND7 to induce ectopic transdifferentiation of Arabidopsis cultured cells into protoxylem vessel-like cells [16].

In this study, we use the VND7 system in Arabidopsis suspension-culture cells because it is a robust model with a high efficiency in transdifferentiation and uniformity in cell culture. To decouple the effects of cell wall stress, cytoskeleton rearrangement, and turgor pressure on observed cell stiffness, we test transgenic Arabidopsis cells in an extensive multi-scale biomechanical assay. We perform micro-compression experiments on isolated cells in three osmotic conditions. We test cells (i) in growth medium to probe their properties in normal growth (isotonic) conditions, (ii) in water, a hypotonic condition, to amplify the effect of turgor pressure on the PCW stiffness, (iii) in sorbitol, a hypertonic solution to plasmolyze the cells and deconvolute the response of the cell wall from turgor pressure. To validate the cell wall stiffness decoupled from turgor pressure, we perform AFM indentations [24]. From the measured stiffnesses of plasmolyzed cells, we are reporting for the first time that the SCW is stiffer than the PCW before and after differentiation is induced. We propose a mechanistic spring model to represent the stiffness of the cell in compression, which allows the decoupling of stiffness contributions from the cell wall(s) and cytoplasm. Based on our model and measurements, we report evidence that turgor pressure supplies most of the overall stiffness of the cell, partially through prestressing the PCW. This is in agreement with the findings of Routier-Kierzkowska et al. and many others who have studied the effects of turgor pressure on cell and tissue mechanics [12,25,26]. To investigate the organization of the cytoskeleton during differentiation we compare stiffnesses of the cells measured before and after induction of differentiation. Indeed, as previously observed in treated Arabidopsis protoplasts, the reorganization of the cytoskeleton upon induction of differentiation causes a significant increase in the overall stiffness of the cell [27]. This finding highlights the mechanical contribution of the fibrillar cytoskeleton, and is observed for the first time in an intact cell.

2. Results and Discussion

2.1. Morphological observations of the VND7-inducible Arabidopsis cells

The VND7-inducible Arabidopsis cells were stained and observed under a laser scanning confocal microscope at various stages of their differentiation. We document that transdifferentiation of VND7-inducible cells follows the same general stages as TE differentiation seen in other plant systems [21–23]. From the transmitted and confocal fluorescent images, we can identify three distinct stages of cell transdifferentiation based on the cell wall, as presented in Fig. 1A-F. Using the confocal fluorescent images, we compile three-dimensional reconstructions for each identifiable stage of transdifferentiation,

Preprints (www.preprints.org) | NOT PEER-REVIEWED | Posted: 4 November 2020 doi:10.20944/preprints202011.0188.v1

presented in Fig. 1G-I, which allow the evaluation of the PCW thickness, as well as visualization of the bundled SCW thickenings.

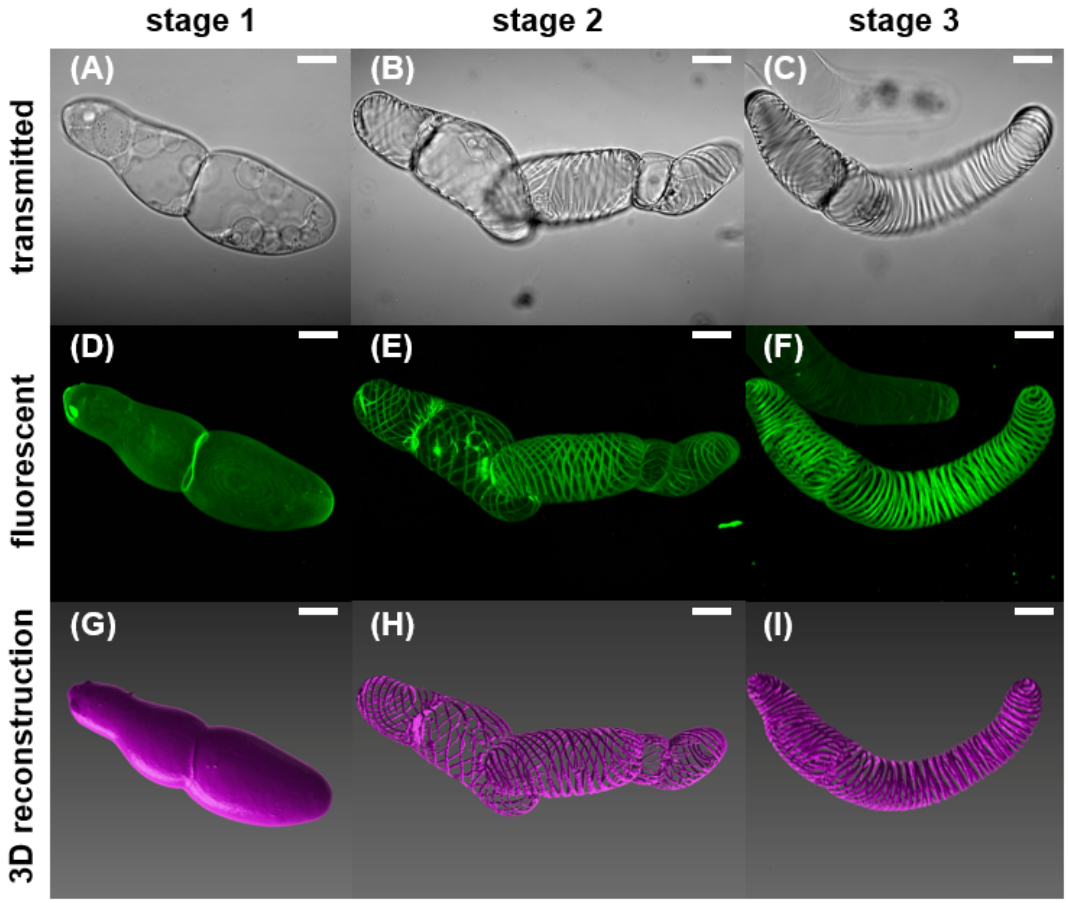

Figure 1. Transmitted, fluorescent, and 3D reconstructions of confocal images of the elongated VND7-inducible cells in the 3 stages of transdifferentiation. (A), (D) & (G) Living cells which have only developed a PCW are identified as stage 1. The PCW is under stress from the internal turgor pressure. (B), (E) & (H) Cells in stage 2 have both a PCW and the beginnings of a SCW. In this stage, the PCW has possibly begun hydrolyzing, and thin spiral bundles of SCW can be distinguished. The spiral patterning is characteristic of protoxylem vessels. (C), (F) & (I) In stage 3, SCW thickening is observed; PCD has progressed; the tonoplast has ruptured and is removed from the cell; partial PCW perforation is visible. All scale bars are 20 μm.

From confocal and additional light microscopy images (data not presented here), we discern two equally represented shapes in the cell population, based on their aspect ratio: rounded and elongated. Elongated cells have a mean aspect ratio of approximately 2:1, whereas rounded cells have a mean aspect ratio of approximately 1:1. Even though the microscopy images denote that approximately half of the population of cells are rounded, and half are elongated, we observe that rounded cells tend to be tightly clustered, while elongated cells are found more likely in an isolated state or located on the edges of large clusters. The mean principal dimensions and standard errors for each shape are reported in Table 1.

The confocal analysis reveals that in stage 1, the PCW thickness of rounded and elongated cells is the same, measured at 580 ± 10 nm in both cases. The population of rounded cells that have transitioned into stage 2 and have deposited SCW bundles, have on average a total cell volume 72% higher than rounded cells at stage 1. Cells that are found to be in stage 3, with fully developed SCW and ruptured tonoplast, have on average an insignificantly changed total volume, compared to cells at stage 2. Our observations indicate a different trend in elongated cells. In that case, the volume of

Preprints (www.preprints.org) | NOT PEER-REVIEWED | Posted: 4 November 2020 doi:10.20944/preprints202011.0188.v1

cells in stages 1 and 2 is almost the same. Between elongated cells in stages 2 and 3, we notice that cells at the last stage of differentiation are about 35% on average larger in volume. The higher volume of cells in stage 3, reflects larger dimensions in both the lateral (11% average increase in width) and longitudinal directions (9% average increase in length). Comparing the volumes of the two shapes, elongated cells are approximately 69% larger than rounded cells in stage 1. In stage 2, elongated and rounded cells have similar volumes. Finally, in stage 3, elongated cells have 22% more volume than rounded cells on average. Apparently, rounded cells are able to enlarge more significantly than elongated cells just prior to SCW deposition.

Table 1. Principal dimensions of elongated and round shaped cells. Length, width and diameter were measured from light microscopy images. Volumes were calculated using formula for a cylinder for elongated cells and a sphere for round cells. The data shown correspond to Mean $\pm$ Standard Error (SE) ($n > 20$).

Cell Shape & Stage	Dimension	Mean $\pm$ SE
Elongated Stage 1	Length (μm)	60.4 ± 2.4
Elongated Stage 2	Length (μm)	56.4 ± 4.9
Elongated Stage 3	Length (μm)	61.6 ± 3.7
Elongated Stage 1	Width (μm)	30.7 ± 1.0
Elongated Stage 2	Width (μm)	31.2 ± 2.8
Elongated Stage 3	Width (μm)	34.7 ± 1.6
Round Stage 1	Diameter (μm)	37.0 ± 0.9
Round Stage 2	Diameter (μm)	44.2 ± 2.1
Round Stage 3	Diameter (μm)	45.0 ± 2.0
Elongated Stage 1	Volume (μm^3)	44700 ± 2100
Elongated Stage 2	Volume (μm^3)	43100 ± 5300
Elongated Stage 3	Volume (μm^3)	58300 ± 4100
Round Stage 1	Volume (μm^3)	26500 ± 1000
Round Stage 2	Volume (μm^3)	45500 ± 3300
Round Stage 3	Volume (μm^3)	47700 ± 3400

Bundles of SCW in spiral patterns are observed in stages 2 and 3 of transdifferentiation. In stage 2, the early SCW bundles are deposited, and the cell begins to undergo PCD. In Table 2 we present the thickness and areal densities of SCW bundles in rounded and elongated cells. We measure that the elongated and rounded cells have similar bundle densities and thicknesses in stage 2. In stage 3, as PCD progresses, the SCW bundles are thickened further, the tonoplast ruptures, contents of the cytoplasm are degraded, and the PCW is at least partially hydrolyzed [2]. We observe that the SCW thickening during the last stage of differentiation leads to the same bundle thickness in both elongated and rounded cells. In both cases the SCW thickens by approximately 40%, as presented in Table 2. The bundle density does not change significantly between stages 2 and 3 for either elongated or rounded cells. The measured bundle density is about 7% higher for elongated cells than for rounded cells. We propose that this is a result of the inherent structural requirement of elongated vessels to be able to support higher stresses in their walls than spherical vessels when experiencing the same amount of pressure.

Preprints (www.preprints.org) | NOT PEER-REVIEWED | Posted: 4 November 2020 doi:10.20944/preprints202011.0188.v1

Table 2. SCW bundle feature sizes for rounded and elongated VND7-inducible cells. Bundle densities were measured from optical microscopy images. Bundle thicknesses were measured from confocal three-dimensional reconstructions. The data shown correspond to Mean ± Standard Error (SE) (n > 45).

Cell Shape & Stage	Dimension (μm)	Mean ± SE
Elongated Stage 2	bundle density (#/μm^2)	0.056 ± 0.005
Elongated Stage 3	bundle density (#/μm^2)	0.060 ± 0.004
Round Stage 2	bundle density (#/μm^2)	0.051 ± 0.005
Round Stage 3	bundle density (#/μm^2)	0.050 ± 0.008
Elongated Stage 2	bundle thickness (μm)	1.05 ± 0.01
Elongated Stage 3	bundle thickness (μm)	1.45 ± 0.01
Round Stage 2	bundle thickness (μm)	1.09 ± 0.04
Round Stage 3	bundle thickness (μm)	1.52 ± 0.03

2.2. *Biomechanics of differentiating VND7-inducible Arabidopsis cells*

We observe that cells of the rounded shape are predominantly found in a clustered state, and cannot be readily isolated to allow single cell compression experiments. Therefore, all reported mechanical data in the following sections are measured from elongated cells, which are more commonly found in an isolated state. In the mechanical testing we add stage 0 to the differentiation stages, which describes transgenic cells prior to exposure to DEX, reflecting cells in their state before transdifferentiation is induced. There is no observable difference between stages 0 and 1 using the confocal or light microscope, but it has been reported that from stage 0 to 1, the MT and actin filaments reorganize the cytoplasmic fibrillar network into a bundled conformation that will later guide the spiral SCW patterning [28,29].

The elongated cells were compressed using a micro-compression tool that covered most of their top surface area. We propose a spring model to describe the overall cell stiffness, as pictured in Fig. 2. The model has two springs in series, one which represents the stiffness of the cell wall, and one which represents the stiffness of the cytoplasm. This model allows us to decouple the stiffness of each component to an extent. See Fig. A1 for the specific spring models used to represent cells in each stage of transdifferentiation, and in each osmolarity of solution.

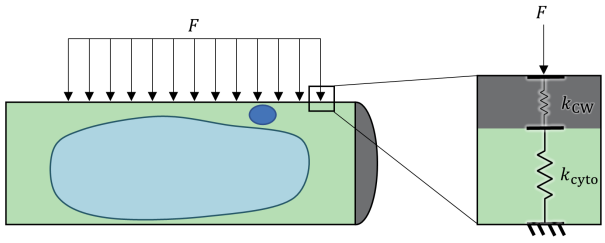

Figure 2. Proposed spring model to analyze cell stiffness from micro-compression testing.

For the micro-indentation tests, we extract cells from their normal growth conditions at different time points before and after exposure to DEX, thereby capturing them at each of the three identified differentiation stages. After the extraction from normal growth conditions, prior to the mechanical testing, we treat the cells in three different osmotic conditions, and maintain these conditions during mechanical testing. In Fig. 3 the initial effective stiffness values for the overall cell in each stage of differentiation, are presented grouped by osmolarity of solution. Underneath each category is a graphical illustration of the morphology of the cells. See Fig. A2 for an alternative grouping of the stiffness measurements by stage and osmolarity of solution.

Preprints (www.preprints.org) | NOT PEER-REVIEWED | Posted: 4 November 2020 doi:10.20944/preprints202011.0188.v1

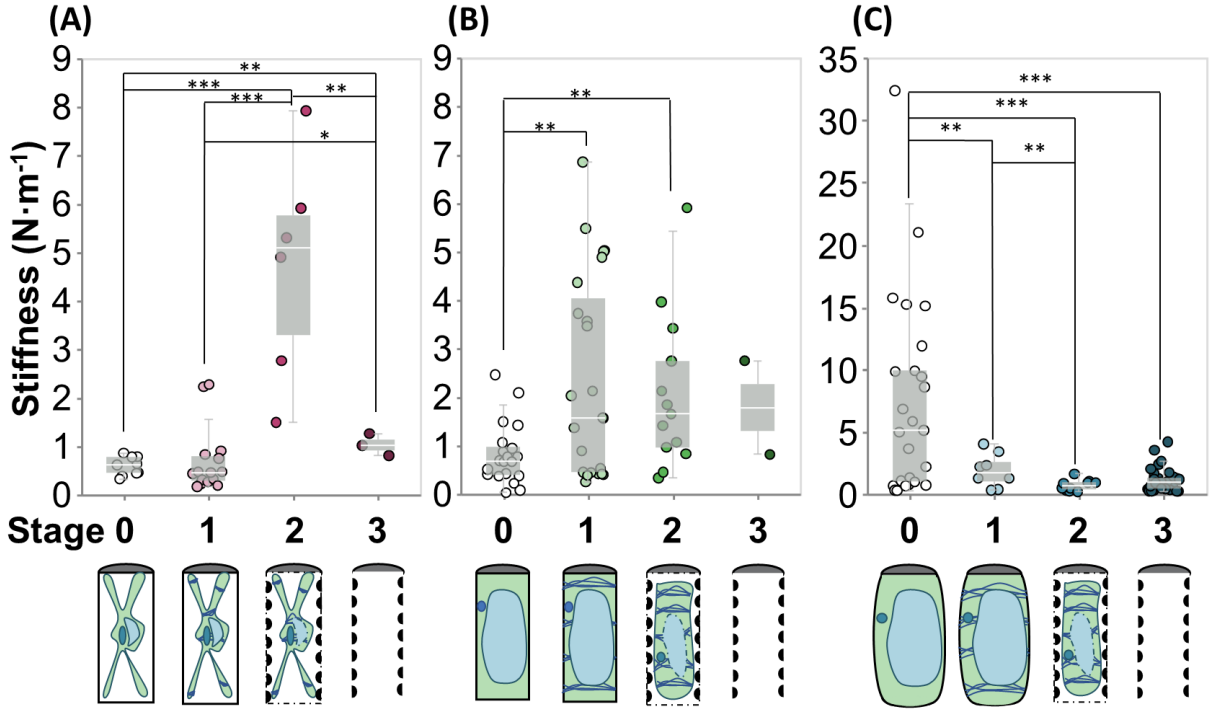

Figure 3. Panel showing the stiffness in 4 stages of transdifferentation in 3 types of solutions with different osmolarity: (A) sorbitol; (B) growth medium; (C) water. Note the difference in scale on the y-axis in (C) from the extreme stiffness of cells in hypotonic conditions before induction of differentiation. Bottom line graphically represents the morphology of the cells in each condition and stage. Stars indicate significant differences in distribution according to the nonparametric Kolmogorov-Smirnov test. * p<0.1, **p<0.05, *** p<0.01. (Data shown correspond to 2<n<35, each represented by a point in the plot.)

2.2.1. Hypertonic Condition

In hypertonic conditions, i.e. the sorbitol condition (Fig. 3A), water flows out of the vacuole and across the cell membrane, as the cell is plasmolyzed. The relief of turgor pressure allows for isolation of the mechanical response of the cell wall [9,30]. When uninduced cells (stage 0) are placed in hypertonic conditions, the measured stiffness ($k_{\text{hyper,stage 0}} = 0.59 \pm 0.06$ N/m) corresponds to that of unstressed PCW.

$$k_{\text{hyper, stage 0}} = k_{\text{PCW}} \tag{1}$$

After DEX exposure, but before the formation of the SCW begins, we do not expect to see a difference in the stiffness of the PCW. Indeed, we do not detect any statistically significant difference in stiffness between stages 0 and 1 in hypertonic conditions ($k_{\text{hyper,stage 1}} = 0.69 \pm 0.17$ N/m). Therefore, we will assume henceforth that induction of transdifferentiation does not cause any change in the stiffness of the PCW.

$$k_{\text{hyper, stage 1}} = k_{\text{PCW}} \tag{2}$$

In stage 2, the PCW is expanded and modified to allow space for the deposition of the SCW [20]. The coupled stiffness of the thin SCW bundles and the modified PCW interact in a way that produces a significant increase on the cellular effective stiffness ($k_{\text{hyper,stage 2}} = 4.71 \pm 2.31$ N/m); this value is over five times the value observed in the prior stages. We propose two possible reasons for the observed increase in stiffness.

Preprints (www.preprints.org) | NOT PEER-REVIEWED | Posted: 4 November 2020 doi:10.20944/preprints202011.0188.v1

The presence of sorbitol may cause an increase of the cell wall stiffness through enhanced molecular interactions between the polysaccharide chains of the PCW and SCW. We hypothesize that in the presence of sorbitol, a polyalcohol with six hydroxyl groups per molecule, these side groups can interact with the available surface hydroxyl groups of the various polysaccharide chains (i.e. cellulose, hemicellulose, pectin) in the PCW and SCW. These polysaccharides are present on each cell wall in different amounts and configurations, and the interactions between them are a topic of active investigations [31]. The introduction of sorbitol may therefore contribute additional hydrogen bonding between the PCW and SCW, supporting our micro-indentation experimental observations.

Alternatively, the collapse of the cell in hypertonic conditions may cause buckling or folding of the PCW over the SCW bundles. Cell wall buckling or folding would result in more amount of cell wall material being compressed under the indenter, thereby justifying a higher stiffness. This apparent stiffening in plasmolyzing conditions due to cell wall buckling has been suggested also for plant tissue indentations [30]. Again, this phenomenon would exist in all stages, but would be enhanced when the PCW is in contact with the spiral SCW. The gaps between the spiral SCW bundles provide channels in between which the PCW could fold, giving the overall cell wall material a thicker and more organized shape.

These two proposed mechanisms for stiffening are not mutually exclusive. The sorbitol may be interacting with cellulose in the PCW as it buckles to provide an even further increase in stiffness for the reorganized overall cell wall structure. In any case, the combined cell walls (CCWs) are the material which provides stiffness to the cell in the hypertonic condition.

$$k_{\text{hyper, stage 2}} = k_{\text{hyper, CCW}} \tag{3}$$

As PCD proceeds, all contents of the cytoplasm are lost and the PCW is hydrolyzed. When the cell is completely differentiated, the main remaining structural component of the xylem vessel element is a thickened SCW. In the final stage, in all solutions, we attribute all the measured stiffness to the thickened SCW ($k_{\text{hyper,stage 3}} = 1.03 \pm 0.13$ N/m).

$$k_{\text{hyper, stage 3}} = k_{\text{SCW}} \tag{4}$$

We measure a statistically significant higher stiffness in stage 3 when compared to stages 0 and 1 in hypertonic conditions. This result suggests that the fully developed SCW is stiffer than the PCW before and after induction.

2.2.2. Isotonic Condition

In isotonic conditions (Fig. 3B), the pressure from the vacuole is in equilibrium with the osmotic pressure from the solution. So, the overall cell shape is not swollen nor shriveled. Turgor pressure from the vacuole and the non-bundled cytoplasm provide additional mechanical stiffness to the cell underneath the cell wall. They are represented by a new spring ($k_{\text{n-b,iso}}$) in our model connected in series to the cell wall(s). Before programmed cell death is initiated, in stages 0 and 1, due to the presence of turgor pressure, we expect the stiffness of the PCW to be higher because it is stressed ($k_{\text{sPCW}} > k_{\text{PCW}}$).

In stage 0, before transdifferentiation is initiated, we observe the lowest stiffness among the cells tested in isotonic solution ($k_{\text{iso,stage 0}} = 0.82 \pm 0.52$ N/m). From our spring model, the overall stiffness of the cell in isotonic conditions in stage 0 is

$$k_{\text{iso, stage 0}} = \frac{k_{\text{sPCW}}(k_{\text{n-b,iso}})}{k_{\text{sPCW}} + k_{\text{n-b,iso}}} \tag{5}$$

There is no statistically significant difference between the effective stiffness of cells in stage 0 in hypertonic and isotonic conditions. For the effective spring constants in both of these models to be

Preprints (www.preprints.org) | NOT PEER-REVIEWED | Posted: 4 November 2020 doi:10.20944/preprints202011.0188.v1

equivalent, the two springs in series in isotonic model must be stiffer than the single spring in the hypertonic model. This implies that the PCW and the combined cytoplasm and vacuole in isotonic conditions must be stiffer than the PCW in hypertonic conditions. In other words, our model confirms that the PCW is stiffened through stress exerted from turgor pressure that exists in isotonic conditions.

Upon induction of transdifferentiation, the effective stiffnesses of the cells are increased significantly. In stage 1, the model still contains 2 springs: one for the stressed PCW (k_{sPCW}), and one for the bundled cytoplasm in isotonic conditions ($k_{\mathrm{b,iso}}$). The mean effective stiffness in stage 1 is $k_{\mathrm{iso,stage\,1}} = 2.40 \pm 0.52$ N/m. Assuming that there is no change in the PCW stiffness from stages 0 to 1, as observed in sorbitol (Fig. 3A), our model indicates that the cytoplasmic contribution in stages 0 must be less than in stage 1 in isotonic conditions ($k_{\mathrm{n\text{-}b,\,iso}} < k_{\mathrm{b,\,iso}}$).

As transdifferentiation proceeds to stage 2, a series of concurrent events influence the mechanical behavior of the cells: (i) the PCW is modified (loosened to allow for elongation for the SCW deposition and possibly entering the hydrolysis stage) (ii) the beginnings of SCW bundles are deposited, and (iii) the anisotropic fibrillar cytoplasm is detached from the cell walls as the turgor pressure is reduced as a result of the cell entering the programmed cell death stage upon differentiation [20]. The stiffness of the new CCW is represented in the spring model as $k_{\mathrm{iso,\,CCW}}$, and the spring from the cytoplasm is removed, since the cytoplasm is no longer in contact with the cell wall. These mechanisms act together to determine the effective stiffness of the cell ($k_{\mathrm{iso,stage\,2}} = 2.06 \pm 0.44$ N/m). The reduced turgor pressure, loss of cytoplasmic contribution as the cell dies and the PCW loosening reduce the effective stiffness of the system. The deposition of SCW increases the stiffness of the cell wall spring component, and therefore the overall system. According to our experiments, the cells have the same stiffness in stages 1 and 2. Thus, if the cytoplasmic contribution is negligible at stage 2, the sPCW of stage 1 must be stiffer than the CCW of stage 2 ($k_{\mathrm{iso,\,CCW}} < k_{\mathrm{sPCW}}$). This highlights the significant effects of turgor pressure stiffening the PCW ins stages 0 and 1.

$$k_{\mathrm{iso,\,stage\,2}} = k_{\mathrm{iso,\,CCW}} \tag{6}$$

At the last stage of differentiation when the SCW is fully developed and thickened, the measured effective stiffness highlights the increased stiffness of a fully developed SCW compared to the PCW ($k_{\mathrm{iso,stage\,3}} = 1.78 \pm 0.97$ N/m).

$$k_{\mathrm{iso,\,stage\,3}} = k_{\mathrm{SCW}} \tag{7}$$

2.2.3. Hypotonic Condition

In water (Fig. 3C), before the DEX induction, we measure the absolute stiffest cell response ($k_{\mathrm{hypo,\,stage\,0}} = 7.37 \pm 1.58$ N/m), which demonstrates that in hypotonic conditions, turgor pressure is the key component for stiffening the overall mechanical response of the cell. The high turgor pressure stresses the PCW to a larger extent than in isotonic conditions ($k_{\mathrm{SPCW}} > k_{\mathrm{sPCW}}$).

$$k_{\mathrm{hypo,\,stage\,0}} = \frac{k_{\mathrm{SPCW}}(k_{\mathrm{n\text{-}b,hypo}})}{k_{\mathrm{SPCW}} + k_{\mathrm{n\text{-}b,hypo}}} \tag{8}$$

SPCW stiffness must be greater than any unstressed CW (primary and/or secondary) because the overall stiffness of cells in hypotonic condition in stage 0 is greater than the overall stiffness in any other case.

As differentiation begins, the overall stiffness of the cell ($k_{\mathrm{hypo,\,stage\,1}} = 1.89 \pm 0.48$ N/m) is drastically reduced. Stress in the PCW is reduced as the PCW prepares for SCW deposition ($k_{\mathrm{SPCW}} > k_{\mathrm{wPCW}}$). Loosening of the PCW to prepare for elongation prior to addition of PCW material has been previously reported, and here we propose that this same mechanism governs SCW deposition [4]. Our analysis could not distinguish the stiffness of the PCW in water stage 1 (k_{wPCW}) from the stiffness of the PCW in growth medium at the same stage (k_{sPCW}).

Preprints (www.preprints.org) | NOT PEER-REVIEWED | Posted: 4 November 2020 doi:10.20944/preprints202011.0188.v1

$$k_{\text{hypo, stage 1}} = \frac{k_{\text{wPCW}}(k_{\text{b,hypo}})}{k_{\text{wPCW}} + k_{\text{b,hypo}}} \tag{9}$$

As SCW is deposited, we measure that the effective stiffness at stage 2 is the lowest among all stages in hypotonic treatment ($k_{\text{hypo, stage 2}} = 0.71 \pm 0.14$ N/m). As seen before, the balance between PCW modification (loosening/hydrolysis), early SCW deposition, and loss of turgor and cytoplasmic contribution determines the overall system stiffness. One possibility for the difference in stiffness between growth medium and water in stage 2 is that the hydrolysis and degradation of PCW may proceed faster in water treatment than in the growth media.

$$k_{\text{hypo, stage 2}} = k_{\text{hypo, CCW}} \tag{10}$$

Finally in the last stage the measured stiffness ($k_{\text{hypo, stage 3}} = 1.12 \pm 0.15$ N/m) corresponds solely to the fully developed SCW. Our results indicate that the combined CW stiffness of stage 2 is weaker than the mature SCW ($k_{\text{hypo, CCW}} < k_{\text{SCW}}$).

$$k_{\text{hypo, stage 3}} = k_{\text{SCW}} \tag{11}$$

As expected, we measure that the thickened SCW in any solution has the same stiffness, which shows that the properties of the fully developed SCW are not affected by the treatments. We have two cases of exceptionally high stiffness; uninduced cells in hypotonic conditions and plasmolyzed cells in stage 2 of transdifferentiation. Besides these two exceptional cases, the SCW alone is at least as stiff as any combined stiffnesses in any other case.

To summarize, the CCW stiffnesses can be ordered as follows:

$$k_{\text{hypo, CCW}} < k_{\text{iso, CCW}} < k_{\text{hyper, CCW}} \tag{12}$$

The proposed molecular mechanisms governing the stiffness of the CCW are the hydrolysis of the PCW in water, and the stiffening of cellulose chains in the presence of sorbitol. Buckling or folding of the PCW in hypertonic conditions may also act to further stiffen the CCW response.

The isolated CW stiffnesses can also be ordered:

$$k_{\text{PCW}} < k_{\text{SCW}} < k_{\text{sPCW}}, k_{\text{wPCW}} < k_{\text{SPCW}} \tag{13}$$

Again, we see that turgor pressure governs the overall mechanical response of the cell to compression through prestressing the PCW. We also confirm that the SCW bundles are stiffer than the PCW material without any prestress.

Finally, the stiffness representing the cytoplasm can be constrained with two inequalities:

$$k_{\text{n-b, iso}} < k_{\text{b, iso}} < k_{\text{n-b,hypo}} \tag{14}$$

$$k_{\text{n-b, iso}} < k_{\text{b, hypo}} \tag{15}$$

The hypotonic condition governs the stiffness of the cytoplasm, before or after the DEX induction, through swelling of the vacuole. In isoosmotic conditions, we observe a stiffening of the cytoplasm upon induction as the MTs and actin filaments bundle to prepare for SCW deposition on the plasma membrane. See Fig. A3 for a visual representation of the magnitude of each stiffness component. Therefore, our assay allows us to directly assess, for the first time, the mechanical contributions of the cytoskeleton in the effective stiffness of intact plant cells, highlighting their important role in the mechanics of the system.

Preprints (www.preprints.org) | NOT PEER-REVIEWED | Posted: 4 November 2020 doi:10.20944/preprints202011.0188.v1

2.3. AFM analysis of differentiating VND7-inducible Arabidopsis cells

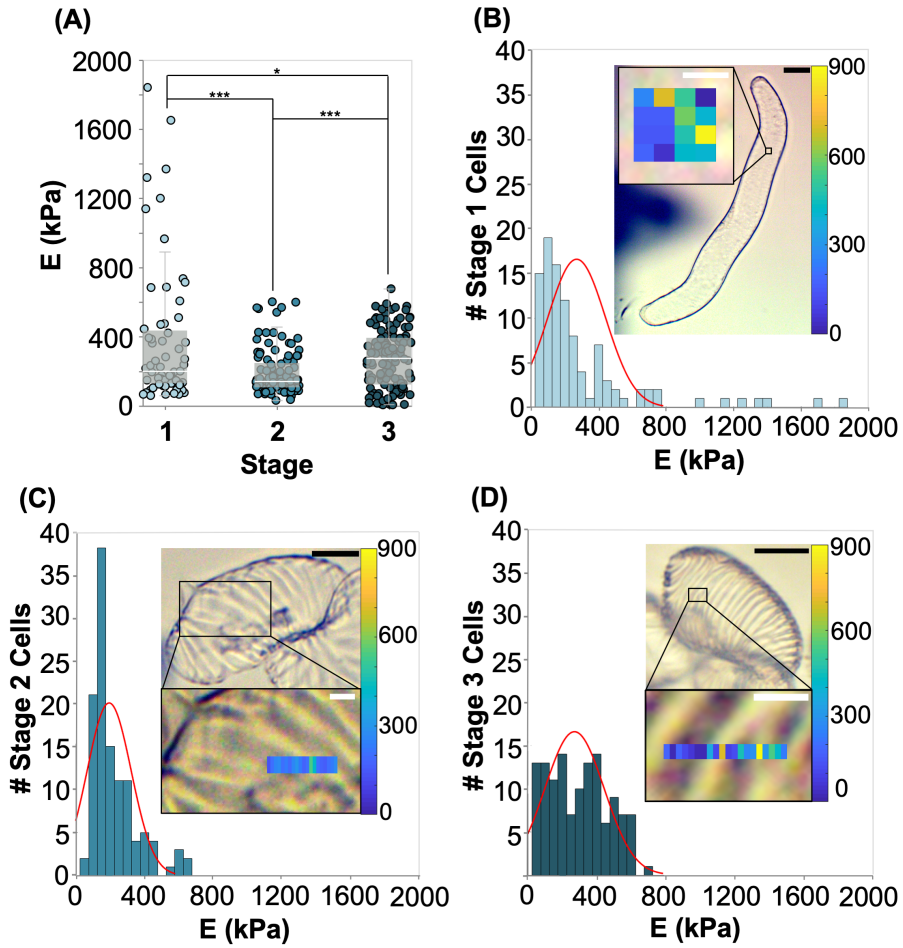

Figure 4. (A) Young's modulus for differentiating VND7-inducible Arabidopsis cells in each stage of differentiation measured with AFM. Stars indicate significant differences in distribution according to a Kolmogorov-Smirnov test. * p<0.1, **p<0.05, *** p<0.01. (Data shown correspond to n>60, each represented by a point in the plot.) (B) Histogram of Young's moduli measured in stage 1 of differentiation. Inset shows example location of measurement and map of stiffness in the area. (C) Histogram of Young's moduli measured in stage 2 of differentiation. Inset shows example location of measurement on cell and line map of stiffness in the area. (D) Histogram of Young's moduli measured in stage 3 of differentiation. Inset shows example location of measurement on cell and line map of stiffness in the area. Inset image scale bars are 20 μm (black). Zoomed-in inset scale bars are 2 μm (white).

AFM nanoindentation tests were conducted in water to evaluate cell wall indentation moduli in each stage of differentiation, as shown in Fig. 4. We use a spherical bead with a 1 μm diameter, which is able to capture the response of a rather large representative area of the PCW, considering the fact that cellulose fibrils are organized in bundles with 5-50 nm thickness [3]. Young's moduli measured from the PCW in stage 1 in hypotonic conditions ($E_{\text{hypo, stage 1}} = 372 \pm 51$ kPa) is higher than in other stages of differentiation, which is in agreement with our micro-indentation results. The Young's moduli measured from the CCW in stage 2 ($E_{\text{hypo, stage 2}} = 192 \pm 13$ kPa) is the lowest of the three stages, again confirming our measurements from the micro-indentation test. Finally, the Young's moduli measured in stage 3 ($E_{\text{hypo, stage 3}} = 271 \pm 15$ kPa) has an intermediate stiffness, which further validates our micro-indentation results.

 doi:10.20944/preprints202011.0188.v1

Measurements with AFM illustrate the extremely heterogeneous structure of the CW. In stage 1, where only the PCW is the only CW of the system, the indentation modulus is measured in a range of 58.7 to 1840 kPa as shown in the histogram and map inset of Fig. 4B. This large distribution arises from the heterogeneous, fibrillar structure of the PCW. The distribution of rigid cellulose fibrils in the compliant heterogeneous matrix of polysaccharides, proteins and phenolic compounds, is causing the local distribution of stiffness we observe with AFM. The high stress in the PCW in hypotonic solution leads to a high stress in the fibres of the PCW, which amplifies the observed heterogeneous stress distribution. In stage 2, the indentation modulus is measured in a range of 31.0 to 601 kPa (Fig. 4C). The higher number of measurements with low moduli in stage 2 illustrate the degradation of the PCW, especially between SCW bundles, which was also suggested from the micro-compression tests. The overlay of line scan measurements on images of the cell reveals that we observe the higher moduli when testing over the combined early SCW bundles and PCW. In the example shown as an inset in Fig. 4C, we see a modulus of approximately 600 kPa over the SCW bundle, and moduli around 300 kPa between the bundles. In stage 3, the indentation modulus is measured in a range of 5.6 to 676 kPa. The inset of Fig. 4D shows a line scan over an area containing two SCW bundles. The line scan shows that the moduli on top of the bundles is as high as 700 kPa, and between the bundles they are about 150 kPa. The indentation moduli measured in stage 3 are more uniformly distributed between the minimum and maximum values than in stage 2. As the SCW bundles thicken, they become stiffer and eliminate the intermittent spaces, leading to fewer measurements over only degraded PCW.

3. Materials and Methods

3.1. Cell culture and differentiation induction

A suspension culture of transgenic *Arabidopsis thaliana* cells (VND7-inducible line, VND7-VP16-GR) was prepared from T87 cell line as described by [16]. The cells were maintained as callus form by the culture on solid agar medium, and transferred to new medium every 3 weeks. Parts of the callus of VND7-inducible cells were used to initiate a suspension culture, which was passaged weekly and was kept in flasks on a rotary shaker at 130 rpm at 23°C. The VND7-inducible cell suspension was maintained in a modified Murashige and Skoog (MS) medium (Duchefa, Haarlem, Netherlands) supplemented with 87 mM sucrose, 1nM 2,4-dichlorphenoxyacetic acid, 555 nM myo-inositol, 2nm thiamin, 34 nM kanamycin, and 1.5 mM Potassium phosphate. To induce differentiation, dexamethasone (DEX) was introduced to the liquid media at a final concentration of 10 μM. Cells were collected post induction from the cultures at different time points and their stage was classified from their morphological features as mentioned in section 2.1. All chemicals and reactants were purchased from MilliporeSigma (St. Louis, MO).

3.2. Microscopy observations

Cell walls were stained with 0.005% (w/v) calcofluor white and observed under a laser scanning confocal microscope (LSM880, Zeiss, Oberkochen, Germany). Cells were extracted from the culture, immersed in staining solution and imaged without any other treatment. Z-stacks were acquired using a 40X water immersion objective (NA 1.2) and Imaris 9.5 (Bitplane, Zurich, Switzerland) was used for 3D rendering and bundles width determination. Specifically the Imaris Measurement Points module was used to quantify the bundles and the Surface module was used to reconstruct the PCW and SCW.

For light microscopy observations, which were performed to measure the dimensions of the cells, the cell walls of freshly extracted cells from culture were stained with 1 vol% solution of alcian blue in 3 vol% acetic acid, and observed with an AxioScope A1 (Zeiss, Oberkochen, Germany). Image analysis was carried out in ImageJ (http://rsb.info.nih.gov/ij/).

 doi:10.20944/preprints202011.0188.v1

3.3. Mechanical testing

We tested the mechanical properties of the cells in three different osmotic conditions: in pure deionized water, in 1M sorbitol, and in growth media (composition mentioned above).

The micro-compression tests were performed using a FT-MTA02 system equipped with FT-S1000-LAT (liquid design) sensing probes with a 50 x 50 μm^2 square tip (FemtoTools AG, Zurich, Switzerland). The obtained data of the indentations were position-corrected to account for contributions of the system's stiffness. Microscope glass slides (AmScope, Irvine, CA) were cleaned with isopropyl alcohol, surface activated with a high frequency generator for 1 minute (BD-20A, Electro-Technic Products, Chicago, IL), and a thin layer of 0.5 mL of poly-l-lysine was spin coated on top of the slides (SUSS MicroTec, Garching, Germany). Cells were extracted from culture and pipetted on the coated glass slides. The cells were washed several times with the selected treatment solution to effectively decluster them and keep only the ones that adhered better to the substrate. For testing 1-3 mL of the selected solution were added on top of the washed and diluted cells, and force-controlled indentations to 900 μN were conducted by immersing the sensing probe in liquid.

Short-range nano-indentations to evaluate the properties of the cell wall were conducted with AFM (Asylum Research, MFP-3D-Bio, Goleta, CA). For the indentations, we used custom tips with a silicon dioxide spherical particle (diameter $1/mum$) on a silicon nitride (SN) cantilever with a stiffness of 0.6 N/m (Novascan, Boone, IA). The AFM indentations were conducted in dionized water, in glass slides treated as mentioned before for the micro-compression tests. For every tested glass slide the system was allowed to reach thermal equilibrium for 2-3 hours. We conducted force-controlled indentations to 3nN and applied the Hertz model to calculate the indentation modulus, E.

3.4. Analysis

Most of the data processing follows that of Routier-Kierzkowska et al. [12]. First, to account for the compliance of the sensor, a reference measurement is obtained by compressing an area of the glass slide with no cells present for 1-2 μm. The linear indentation part of data are linearly fitted. The sensor stiffness (S) is typically above 200 N/m. All data sets are then transformed by

$$\delta_{\text{corrected}} = \delta - \frac{F}{S} \tag{16}$$

where $\delta_{\text{corrected}}$ is the corrected displacement, δ is the measured displacement, F is the measured force, and S is the sensor stiffness determined by calibration.

Next, we offset the measured force-displacement data so that the average force up until the contact point is zero. The contact point is defined as the point where the force exceeds a user-defined threshold. The force thresholding and offsetting are repeated using increasingly sensitive force thresholds. The final selected threshold value is typically less than 1 um. Then, a Savitsky-Golay moving-window data filter is applied to smooth the data. The window size is 25 data points which are fit to a 2nd order polynomial.

Finally, the first 1 μm of indentation data after the located contact point are linearly fitted. The interpolated slope is taken as the overall stiffness of the cell. The overall stiffnesses of cells are compared between stages of transdifferentiation and between osmolarities of testing solutions. A Kolmogorov-Smirnov statistical test is performed which compares the empirical cumulative distribution functions of each grouping.

All data processing was performed using the Python programming language (Python Software Foundation, https://www.python.org/). All statistical visualizations were created using Altair [32].

4. Conclusions

We designed a multi-scale biomechanical assay to experimentally isolate the mechanical contributions from the cytoplasm and cell wall during the differentiation of transgenic Arabidopsis

 doi:10.20944/preprints202011.0188.v1

cells to protoxylem vessel elements. The combination of mechanical data at different scales and in different osmotic conditions allows us to decouple the contributions from each structural element of the cell as it responds to changes in turgor pressure at various stages of the differentiation process. Our analysis provides experimental evidence that the SCW is stiffer than the relaxed PCW, in a living cell system. This conclusion is reached by comparing measured cell stiffnesses in hypertonic conditions, where the cell wall is effectively decoupled from the cytoplasm. In isotonic and hypotonic conditions, turgor pressure gives rise to an increased stress in PCW, causing it to stiffen beyond the SCW. We also measure a quantifiable loosening of the PCW in stage 1, as the cell prepares for deposition of the SCW. This is the first time a mechanical weakening is measured on the PCW before the SCW deposition in living cells. From measurements in isotonic and hypotonic conditions, we also find evidence of a quantifiable difference in cytoplasmic stiffness as a consequence of active bundling of the filaments in the cytoplasm, guided by differentiation.

These findings provide insight into the mechanisms of xylem vessel element differentiation. They suggest that inter- and/or intra-cellular mechanical signals regulate cell differentiation and SCW deposition.

Author Contributions: conceptualization, E.R., M.O., T.D. and C.D.; methodology, E.R.; data analysis, E.R., L.G., R.M., G.S.; data curation, E.R., L.G.; writing–original draft preparation, E.R., L.G.; writing–review and editing, E.R., L.G., R.M., G.S., R.H., M.O., T.D., G. R, and C.D.; visualization, E.R., L.G., R.M., G.S.

Funding: This work was supported in part by the Resnick Sustainability Institute at Caltech (C.D.) and by the MEXT KAKENHI Grant Numbers JP18H05484 and JP18H05489 (M.O. and T.D.).

Acknowledgments: We would like to acknowledge the contributions of Jenny Martinez, who conducted part of the micro-indentations in water, and Dr. Luca Bonanomi for helpful discussions.

Conflicts of Interest: The authors declare no conflict of interest.

Abbreviations

The following abbreviations are used in this manuscript:

AFM	Atomic-force microscopy
DEX	dexamethasone
PCW	Primary cell wall
SCW	Secondary cell wall
TE	Tracheary element
PCD	Programmed cell death
SE	Standard error

Preprints (www.preprints.org) | NOT PEER-REVIEWED | Posted: 4 November 2020 doi:10.20944/preprints202011.0188.v1

Appendix A

Appendix A.1

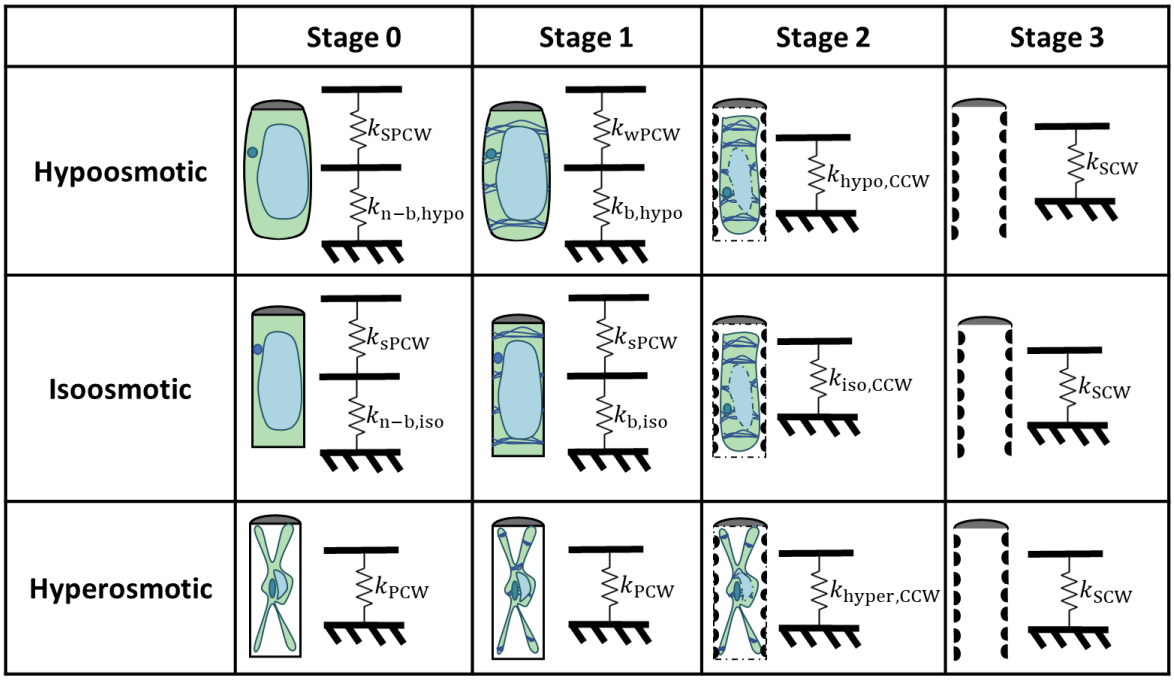

Figure A1. spring models for all treatments/stages

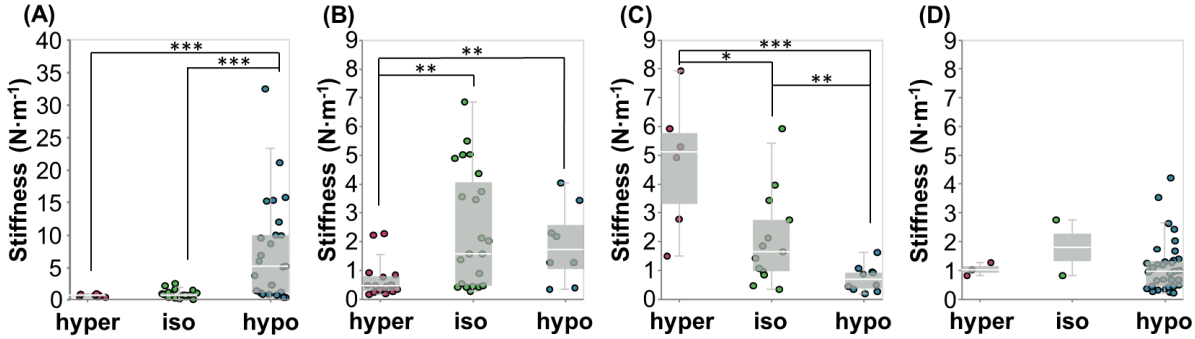

Figure A2. Panel showing stiffness in hypertonic, isotonic, and hypotonic solutions in 4 stages of transdifferentiation: (A) stage 0; (B) stage 1; (C) stage 2; (D) stage 3. Stars indicate significant differences in distribution according to a Kolmogorov-Smirnov test. * p<0.1, **p<0.05, *** p<0.01

 doi:10.20944/preprints202011.0188.v1

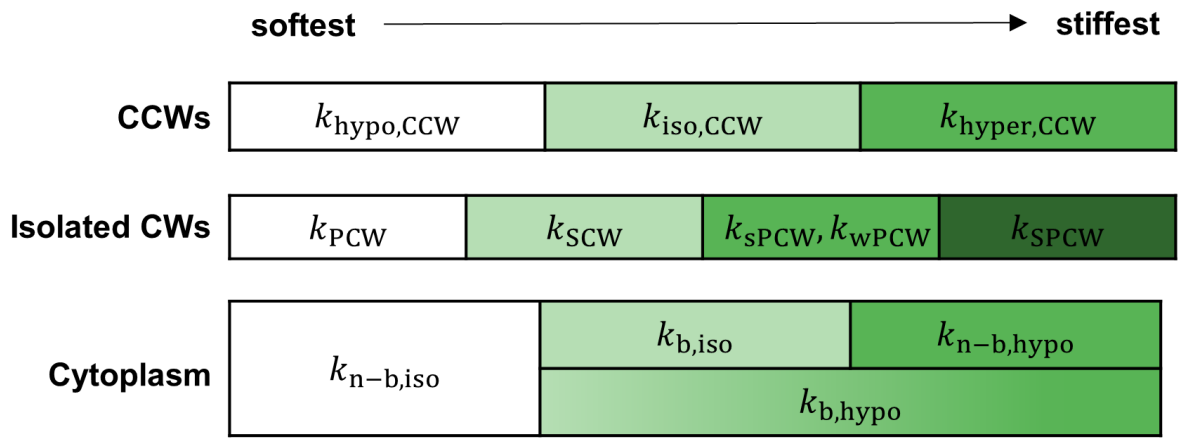

Figure A3. Stiffness comparison for each component of spring models.

1. Gibson, L.J. The hierarchical structure and mechanics of plant materials. *Journal of the royal society interface* **2012**, *9*, 2749–2766.
2. Zhong, R.; Cui, D.; Ye, Z.H. Secondary cell wall biosynthesis. *New Phytologist* **2019**, *221*, 1703–1723, [https://nph.onlinelibrary.wiley.com/doi/pdf/10.1111/nph.15537]. doi:10.1111/nph.15537.
3. Moon, R.J.; Martini, A.; Nairn, J.; Simonsen, J.; Youngblood, J. Cellulose nanomaterials review: structure, properties and nanocomposites. *Chem. Soc. Rev.* **2011**, *40*, 3941–3994. doi:10.1039/C0CS00108B.
4. Cosgrove, D.J. Plant cell wall extensibility: connecting plant cell growth with cell wall structure, mechanics, and the action of wall-modifying enzymes. *Journal of Experimental Botany* **2015**, *67*, 463–476, [https://academic.oup.com/jxb/article-pdf/67/2/463/9366332/erv511.pdf]. doi:10.1093/jxb/erv511.
5. Cosgrove, D.J. Assembly and enlargement of the primary cell wall in plants. *Annual Review of Cell and Developmental Biology* **1997**, *13*, 171–201, [https://doi.org/10.1146/annurev.cellbio.13.1.171]. PMID: 9442872, doi:10.1146/annurev.cellbio.13.1.171.
6. Chaudhuri, O.; Parekh, S.H.; Fletcher, D.A. Reversible stress softening of actin networks. *Nature* **2007**, *445*, 295–298. doi:10.1038/nature05459.
7. Gittes, F.; Mickey, B.; Nettleton, J.; Howard, J. Flexural rigidity of microtubules and actin filaments measured from thermal fluctuations in shape. *Journal of Cell Biology* **1993**, *120*, 923–934, [https://rupress.org/jcb/article-pdf/120/4/923/384296/923.pdf]. doi:10.1083/jcb.120.4.923.
8. Durand-Smet, P.; Chastrette, N.; Guiroy, A.; Richert, A.; Berne-Dedieu, A.; Szecsi, J.; Boudaoud, A.; Frachisse, J.M.; Bendahmane, M.; Hamant, O.; Asnacios, A. A Comparative Mechanical Analysis of Plant and Animal Cells Reveals Convergence across Kingdoms. *Biophysical Journal* **2014**, *107*, 2237 – 2244. doi:https://doi.org/10.1016/j.bpj.2014.10.023.
9. Bidhendi, A.J.; Geitmann, A. Methods to quantify primary plant cell wall mechanics. *Journal of Experimental Botany* **2019**, *70*, 3615–3648, [https://academic.oup.com/jxb/article-pdf/70/14/3615/28985115/erz281.pdf]. doi:10.1093/jxb/erz281.
10. Geitmann, A. Experimental approaches used to quantify physical parameters at cellular and subcellular levels. *American Journal of Botany* **2006**, *93*, 1380–1390, [https://bsapubs.onlinelibrary.wiley.com/doi/pdf/10.3732/ajb.93.10.1380]. doi:10.3732/ajb.93.10.1380.
11. Milani, P.; Braybrook, S.A.; Boudaoud, A. Shrinking the hammer: micromechanical approaches to morphogenesis. *Journal of Experimental Botany* **2013**, *64*, 4651–4662, [https://academic.oup.com/jxb/article-pdf/64/15/4651/18043081/ert169.pdf]. doi:10.1093/jxb/ert169.
12. Routier-Kierzkowska, A.L.; Weber, A.; Kochova, P.; Felekis, D.; Nelson, B.J.; Kuhlemeier, C.; Smith, R.S. Cellular Force Microscopy for in Vivo Measurements of Plant Tissue Mechanics. *Plant Physiology* **2012**, *158*, 1514–1522, [http://www.plantphysiol.org/content/158/4/1514.full.pdf]. doi:10.1104/pp.111.191460.

13. Sampathkumar, A.; Krupinski, P.; Wightman, R.; Milani, P.; Berquand, A.; Boudaoud, A.; Hamant, O.; Jönsson, H.; Meyerowitz, E.M. Subcellular and supracellular mechanical stress prescribes cytoskeleton behavior in *Arabidopsis* cotyledon pavement cells. *eLife* **2014**, *3*, e01967. doi:10.7554/eLife.01967.
14. Radotić, K.; Roduit, C.; Simonović, J.; Hornitschek, P.; Fankhauser, C.; Mutavdžić, D.; Steinbach, G.; Dietler, G.; Kasas, S. Atomic force microscopy stiffness tomography on living Arabidopsis thaliana cells reveals the mechanical properties of surface and deep cell-wall layers during growth. *Biophysical Journal* **2012**, *103*, 386–394. doi:10.1016/j.bpj.2012.06.046.
15. Braybrook, S.A.; Peaucelle, A. Mechano-Chemical Aspects of Organ Formation in Arabidopsis thaliana: The Relationship between Auxin and Pectin. *PLOS ONE* **2013**, *8*, 1–10. doi:10.1371/journal.pone.0057813.
16. Yamaguchi, M.; Goué, N.; Igarashi, H.; Ohtani, M.; Nakano, Y.; Mortimer, J.C.; Nishikubo, N.; Kubo, M.; Katayama, Y.; Kakegawa, K.; Dupree, P.; Demura, T. VASCULAR-RELATED NAC-DOMAIN6 and VASCULAR-RELATED NAC-DOMAIN7 Effectively Induce Transdifferentiation into Xylem Vessel Elements under Control of an Induction System. *Plant Physiology* **2010**, *153*, 906–914. Publisher: American Society of Plant Biologists Section: BREAKTHROUGH TECHNOLOGIES, doi:10.1104/pp.110.154013.
17. Kubo, M.; Udagawa, M.; Nishikubo, N.; Horiguchi, G.; Yamaguchi, M.; Ito, J.; Mimura, T.; Fukuda, H.; Demura, T. Transcription switches for protoxylem and metaxylem vessel formation. *Genes & Development* **2005**, *19*, 1855–1860, [http://genesdev.cshlp.org/content/19/16/1855.full.pdf+html]. doi:10.1101/gad.1331305.
18. Yin, Z.; Fan, R. Ultrastructural analysis of the differentiation process of secondary xylem vessel element in *Populus deltoides*. *Frontiers of Forestry in China* **2009**, *4*. Publisher: Springer, doi:10.1007/s11461-009-0067-6.
19. Meents, M.J.; Watanabe, Y.; Samuels, A.L. The cell biology of secondary cell wall biosynthesis. *Annals of Botany* **2018**, *121*, 1107–1125, [https://academic.oup.com/aob/article-pdf/121/6/1107/24805712/mcy005.pdf]. doi:10.1093/aob/mcy005.
20. Bollhöner, B.; Prestele, J.; Tuominen, H. Xylem cell death: emerging understanding of regulation and function. *Journal of Experimental Botany* **2012**, *63*, 1081–1094. Publisher: Oxford Academic, doi:10.1093/jxb/err438.
21. Fukuda, H. Tracheary Element Differentiation. *The Plant Cell* **1997**, *9*, 1147–1156.
22. Iakimova, E.T.; Woltering, E.J. Xylogenesis in zinnia (Zinnia elegans) cell cultures: unravelling the regulatory steps in a complex developmental programmed cell death event. *Planta* **2017**, *245*, 681–705.
23. Kákošová, A.; Digonnet, C.; Goffner, D.; Lišková, D. Galactoglucomannan oligosaccharides are assumed to affect tracheary element formation via interaction with auxin in Zinnia xylogenic cell culture. *Plant cell reports* **2013**, *32*, 479–487.
24. Vogler, H.; Felekis, D.; Nelson, B.J.; Grossniklaus, U. Measuring the Mechanical Properties of Plant Cell Walls. *Plants* **2015**, *4*, 167–182. doi:10.3390/plants4020167.
25. Weber, A.; Braybrook, S.; Huflejt, M.; Mosca, G.; Routier-Kierzkowska, A.L.; Smith, R.S. Measuring the mechanical properties of plant cells by combining micro-indentation with osmotic treatments. *Journal of Experimental Botany* **2015**, *66*, 3229–3241, [https://academic.oup.com/jxb/article-pdf/66/11/3229/17137090/erv135.pdf]. doi:10.1093/jxb/erv135.
26. Hamant, O.; Haswell, E.S. Life behind the wall: sensing mechanical cues in plants. *BMC Biology* **2017**, *15*, 59. doi:10.1186/s12915-017-0403-5.
27. Durand-Smet, P.; Spelman, T.A.; Meyerowitz, E.M.; Jönsson, H. Cytoskeletal organization in isolated plant cells under geometry control. *Proceedings of the National Academy of Sciences* **2020**, *117*, 17399–17408, [https://www.pnas.org/content/117/29/17399.full.pdf]. doi:10.1073/pnas.2003184117.
28. Oda, Y.; Hasezawa, S. Cytoskeletal organization during xylem cell differentiation. *Journal of Plant Research* **2006**, *119*, 167–177. doi:10.1007/s10265-006-0260-8.
29. Sasaki, T.; Fukuda, H.; Oda, Y. CORTICAL MICROTUBULE DISORDERING1 Is Required for Secondary Cell Wall Patterning in Xylem Vessels. *The Plant Cell* **2017**, *29*, 3123–3139, [http://www.plantcell.org/content/29/12/3123.full.pdf]. doi:10.1105/tpc.17.00663.
30. Braybrook, S.A. Chapter 13 - Measuring the elasticity of plant cells with atomic force microscopy. In *Biophysical Methods in Cell Biology*; Paluch, E.K., Ed.; Academic Press, 2015; Vol. 125, *Methods in Cell Biology*, pp. 237 – 254. doi:https://doi.org/10.1016/bs.mcb.2014.10.006.

31. Watanabe, Y.; Meents, M.J.; McDonnell, L.M.; Barkwill, S.; Sampathkumar, A.; Cartwright, H.N.; Demura, T.; Ehrhardt, D.W.; Samuels, A.L.; Mansfield, S.D. Visualization of cellulose synthases in Arabidopsis secondary cell walls. *Science* **2015**, *350*, 198–203. Publisher: American Association for the Advancement of Science Section: Report, doi:10.1126/science.aac7446.
32. VanderPlas, J.; Granger, B.; Heer, J.; Moritz, D.; Wongsuphasawat, K.; Satyanarayan, A.; Lees, E.; Timofeev, I.; Welsh, B.; Sievert, S. Altair: Interactive Statistical Visualizations for Python. *Journal of Open Source Software* **2018**. doi:10.21105/joss.01057.